

2022-07-15

Distribution and transport of microplastics in groundwater (Shiraz aquifer, southwest Iran)

Esfandiari, A

<http://hdl.handle.net/10026.1/19528>

10.1016/j.watres.2022.118622

Water Research

Elsevier

All content in PEARL is protected by copyright law. Author manuscripts are made available in accordance with publisher policies. Please cite only the published version using the details provided on the item record or document. In the absence of an open licence (e.g. Creative Commons), permissions for further reuse of content should be sought from the publisher or author.

1 **Distribution and transport of microplastics in groundwater (Shiraz**
2 **aquifer, southwest Iran)**

3

4 Atefeh Esfandiari ^a, Sajjad Abbasi * ^{b,c}, Ahmad Behruj Peely ^b, Dariush Mowla ^a, Mohammad
5 Ali Ghanbarian ^b, Patryk Oleszczuk ^c, Andrew Turner ^d

6

7 ^a Environmental Research Centre in Petroleum and Petrochemical Industries, Department of
8 Chemical Engineering, School of Chemical and Petroleum Engineering, Shiraz University,
9 Shiraz, Iran

10 ^b Department of Earth Sciences, College of Science, Shiraz University, Shiraz 71454, Iran

11 ^c Department of Radiochemistry and Environmental Chemistry, Faculty of Chemistry, Maria
12 Curie-Skłodowska University, Lublin 20-031, Poland

13 ^d School of Geography, Earth and Environmental Sciences, University of Plymouth, Plymouth
14 PL4 8AA, UK

15

16

17 * Corresponding author. Department of Earth Sciences, College of Science, Shiraz University, 71454, Shiraz, Iran;

18 Department of Radiochemistry and Environmental Chemistry, Faculty of Chemistry, Maria Curie-Skłodowska

19 University, Lublin 20-031, Poland. E-mail address: sajjad.abbasi.h@gmail.com; sajjad.abbasi@shirazu.ac.ir

20

21 **Accepted 13 May 2022**

22

23 <https://doi.org/10.1016/j.watres.2022.118622>

24

25

26

27

28

29

30

31 **Abstract**

32 Despite the significance of groundwater to the hydrological cycle and as a source of potable water,
33 very little information exists on microplastics (MPs) in this environment. In the present study, MPs
34 have been determined in ten well samples obtained from an alluvial aquifer in a semi-arid region
35 (Shiraz, Iran) following filtration, digestion and inspection under a binocular microscope. A total
36 of 96 MPs were identified, and concentrations ranged from 0.1 to 1.3 MP L⁻¹ (mean and median =
37 0.48 and 0.43 MP L⁻¹, respectively) and exhibited a complex distribution across the area that
38 reflected differences in land use and local hydrology and geology. The majority of MPs (about
39 70%) were fibres of $\leq 500 \mu\text{m}$ in length, but fragments and films were present at some sites, and
40 the dominant polymers were polystyrene, polyethylene and polyethylene terephthalate. Coupling
41 meteorological and water table monitoring data from the regional water organization and published
42 information on aquifer hydrology, we estimate a lag time from precipitation to water table intrusion
43 of between one and five months and groundwater velocity flows of between 0.01 and 0.07 m d⁻¹.
44 Although the extent of retardation of MPs within the pores of groundwater is unknown, by
45 considering empirical data and theoretical predictions on particle flow through porous media in
46 the literature we surmise that MP residence times in the aquifer are likely to range from months to
47 decades, thereby impeding any clear means of source identification. Nevertheless, and more
48 generally, the consumption of potable groundwater may make to a contribution to MP exposure
49 through ingestion.

50

51

52 **Keywords:** groundwater; fibres; precipitation; transport; hydrogeology; modelling

53

54 **1. Introduction**

55 Groundwater plays a critical role in the hydrological cycle and, in the form of aquifers, is an
56 important water resource. In arid and semi-arid regions, aquifers are particularly valuable for
57 socio-economic development, acting as a source of water for drinking, agriculture and industry
58 (Scanlon et al., 2006; Hssaisoune et al., 2020). However, because of the demands on aquifers in
59 populated areas, abstraction may well exceed recharge and depletion of groundwater takes place.
60 In addition to resource loss, diminishing reserves may be associated with drying of springs,
61 abandonment of wells, increased pumping costs and, depending on local geology, a reduction in
62 water quality (Rodríguez-Estrella, 2012).

63 Inadequate water and waste management and treatment and poor agricultural and industrial
64 practices can also lead to the contamination of groundwater by a variety of substances, with
65 consequences for human health and the local environment and ecosystems. Specifically, excessive
66 applications of agrochemicals can result in high groundwater levels of nitrate, pesticides and
67 potassium (Oren et al., 2004; Abdesselam et al., 2013; El Alfy and Faraj, 2016), while urban runoff
68 and waste water and the use of untreated water for irrigation may adversely impact on levels of
69 chemical oxygen and may introduce road salts, oils, metals, pharmaceuticals and pathogens
70 (Fernández-Cirelli et al., 2009, Abd-Elaty et al., 2021; Li et al., 2021).

71 Another type of contaminant that is both persistent and pervasive is microplastics (MPs), or
72 plastics whose primary diameters are less than 5 mm. The distribution, behaviour, impacts and fate
73 of MPs have been extensively studied in the marine and fresh water environments, and in soils and
74 the atmosphere (da Costa et al., 2018; Ng et al., 2018; Allen et al., 2019; Abbasi and Turner, 2021;
75 Coyle et al., 2021; Tanentzap et al., 2021), but there is very little study of MPs in the subsurface

76 environment. Minteneg et al. (2018) provided evidence for the presence of MPs in groundwater
77 by detecting small quantities ($< 7 \text{ MP m}^{-3}$) in groundwater sampled from wells at more than 30 m
78 depth in north west Germany. Panno et al. (2018) found significantly higher concentrations of MPs
79 (up to 15.2 MP L^{-1}) that were all fibrous in nature in springs and wells from two more open karst
80 aquifers in Illinois, USA, and attributed their presence, largely, to septic effluent. Most recently,
81 Samandra et al. (2022) found concentrations of MPs that were mainly fragments and fibres
82 averaging about 40 MP L^{-1} in groundwater sampled from capped monitoring bores in an alluvial
83 aquifer in Victoria, Australia. Because of the abundance of alluvial aquifers globally, the authors
84 called for further research into this type of system.

85 We present the first study of MPs in an alluvial aquifer from a semi-arid region (Shiraz, southwest
86 Iran). High volume samples are taken from a number of observation (monitoring) wells and MPs
87 are isolated, identified and characterized according to established techniques. We also utilize
88 seasonal distributions of rainfall and water table depth for the region to provide a semi-quantitative
89 assessment of the velocities of MPs in groundwater and the timescales that they may reside in the
90 subsurface environment.

91

92 **2. Methods**

93 ***2.1. Study area and hydrogeological characteristics***

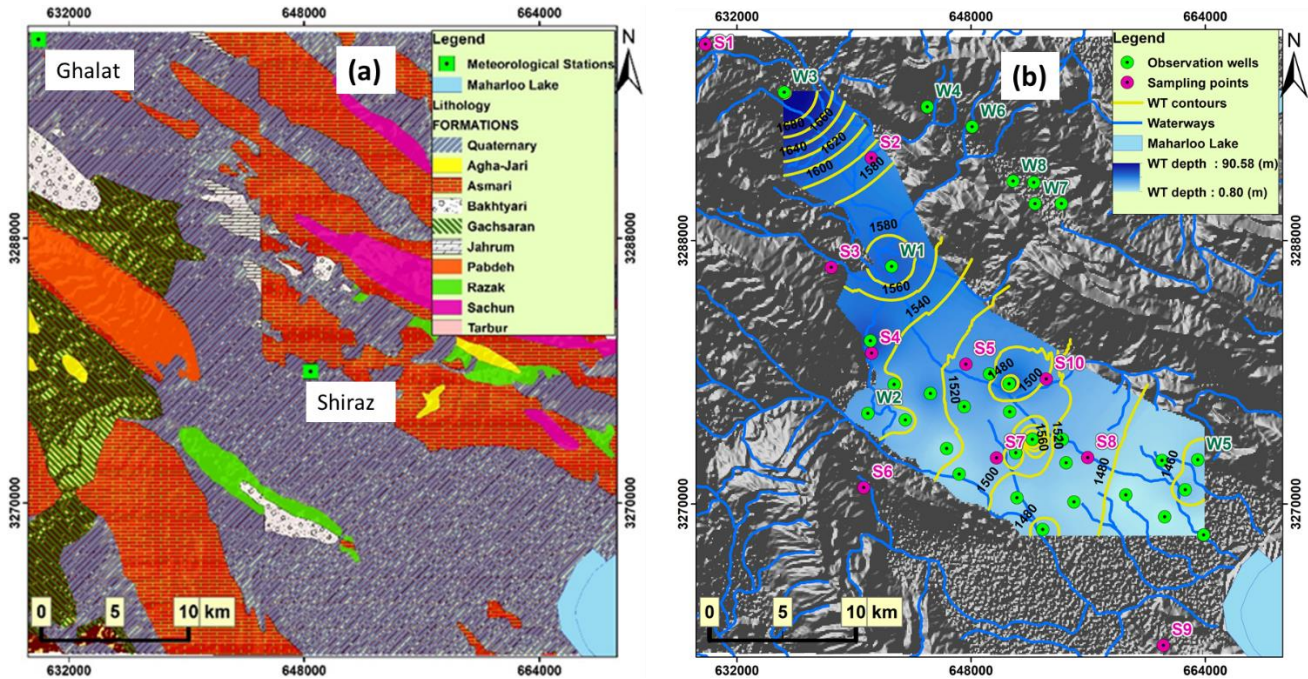
94 The geology and hydrology of the Shiraz watershed and aquifer are shown in Figures 1a and 1b,
95 respectively. Shiraz watershed is located within the Zagros foreland folded belt of the Fars
96 province of southwest Iran and is about 1450 km^2 in area (Jafari et al. 2021), with the highest
97 elevations in the northern reaches (The Ghalat Mountains; about 2900 m) and the lowest elevations

98 towards Maharloo Lake in the south (about 1430 m). Annual average precipitation at Galat and
99 Shiraz meteorological stations is 480 and 354 mm, respectively, with most precipitation falling
100 between the months of November and March. The principal rivers (the Khoshk and its tributary,
101 the Azam) drain the catchment on a seasonal basis and head in a southeasterly direction, passing
102 through Shiraz city and recharging the lake. According to Jafari et al. (2021), land use is dominated
103 by pasture and bare land, with smaller contributions from urban, agriculture, orchard, forest and
104 wetland, and soils are heterogeneous and erosive silty and sandy loams.

105 Shiraz aquifer occupies an area of about 300 km² in the Shiraz watershed and is an unconfined
106 alluvial system surrounded by karstic limestone (and mainly Asmari-Jahrum) formations.
107 Quaternary deposits consist of coarse-grained sediments and medium- to fine-grained clastic
108 materials, but closer to Maharloo Lake sediments become finer and admixed with halite and
109 gypsum (Tajabadi et al., 2018). The aquifer has an average thickness of 30 m where unconfined,
110 and mean water table depth generally ranges from about 35 m to the north and west to < 3 m in
111 the south (where greater evaporation and mixing with lake water results in more saline water;
112 Tajabadi et al., 2018; Jafari et al., 2021). However, because of vertical granulometric variations,
113 confined groundwater can be found at depths exceeding 200 m in some places (Baghapour et al.,
114 2016). The general flow is from the northwest to the southeast, and interactions with the Khoshk
115 River are restricted to the southeast of the aquifer. Land use within the region is mainly residential,
116 cultivated and, towards the lake, barren because of soil salinization (Amiri et al., 2015). Although
117 the region relies heavily on groundwater resources for economic and demographic development,
118 contamination from wastes, and in particular by nitrate from agriculture, present a pervasive
119 problem (Baghapour et al., 2016; Alamdar et al., 2019).

120 The approximate boundary of the aquifer and contours of water table elevation are shown in Figure
121 1b. Water table levels and depths obtained from the Shiraz Regional Water Organization were
122 interpolated using inverse distance weighting (Charizopoulos et al., 2018), with water table
123 elevation contours subsequently extracted from the water table raster file using ArcMap 10.8. Note
124 the decline in water table elevation from over 1700 m in the north to < 1460 m in the south; note
125 also that the southern and eastern boundaries could not be as accurately defined from available
126 data.

127



128

129

130 Figure 1: (a) The geology of the Shiraz watershed, from the Galat Mountains (northwest) to
 131 Maharloo Lake (southeast), illustrating the distribution of Quaternary deposits and surrounding
 132 karstic limestones. (b) The approximate, modelled boundary of Shiraz alluvial aquifer, mean
 133 contours of water table elevation (in m above sea level and at 20 m intervals) and seasonal,
 134 surface waterways. Wells used to map the aquifer are show in green ($n = 32$), with the eight used
 135 for time lag modelling numbered, and wells shown in pink ($n = 8$) are where MPs were sampled
 136 from.

137

138 **2.2. Sample collection**

139 Groundwater samples were obtained from ten wells located throughout Shiraz aquifer (and just
 140 beyond its modelled boundary but within Quaternary deposits) in May 2021 (Figure 1b and Table
 141 1). Wells in the region are open, with flow rates ranging from < 3 to about 90 L s^{-1} . Most are lined
 142 with 10 to 50 cm-diameter stainless steel, but some are lined with black polyethylene. In the
 143 unsaturated zone, liners are supported by and sealed with cement grout, while below this zone,

144 liners are perforated and encased in stainless steel mesh whose pore size is variable (but generally
145 around 1-2 mm) or unknown. At each site, the pump was turned on and water was allowed to flow
146 for about fifteen to thirty minutes in order to minimize contamination from direct atmospheric
147 deposition into the well. Samples of 20 L were then collected in two custom-made ~ 10-L amber
148 glass bottles that had been pre-rinsed with filtered ($< 2 \mu\text{m}$) water by an operator wearing latex
149 gloves and cotton clothing.

150

151 Table 1: Coordinates and elevation of the wells sampled and estimates of mean water table (WT)
152 depth based on interpolation of the contours shown in Figure 1b.

Location	X	Y	elevation, m	WT depth, m
S1	629860	3301408	1984	184
S2	641200	3293634	1740	150
S3	638448	3286167	1771	201
S4	641206	3280305	1594	44
S5	647648	3279552	1569	69
S6	640674	3271120	1561	31
S7	649741	3273149	1516	1
S8	655980	3273165	1492	7
S9	661139	3260341	1471	21
S10	653143	3278537	1585	85

153

154

155 ***2.3. Microplastic extraction and identification***

156 Well waters were processed in a clean facility and using pre-filtered water and reagents and pre-
157 cleaned consumables and glassware as in our previous studies (Abbasi and Turner, 2021). Briefly,
158 250 mL of 30% H_2O_2 (Arman Sina, Tehran) was added to each bottle and the contents were left at
159 room temperature for 7 d. Digests from each location (i.e. two bottles) were then vacuum-filtered
160 through 150 mm diameter S&S filters (Blue Band, grade 589/3, $2 \mu\text{m}$ pore size) using a glass-

161 porcelain Buchner system, and filters were subsequently dried under aluminium foil in a clean
162 cabinet at room temperature for 24 to 48 h.

163 Material on each filter was carefully transferred into a series of glass petri dishes using a fine,
164 horsehair brush and MPs were identified using a binocular microscope (Carl-Zeiss) at up to 200 x
165 magnification with the aid of a 250 μm -diameter stainless steel probe and ImageJ software.
166 Identification was based on shininess, cross-sectional properties, surface structure, thickness,
167 hardness and reaction to the heated probe and according to criteria given by Hidalgo-Ruz et al.
168 (2012) and De Witte et al. (2014). Particle size was classified in terms of the longest dimension
169 or, for fibres, length, L , as $\leq 100 \mu\text{m}$, $100 < L \leq 250 \mu\text{m}$, $250 \leq L < 500 \mu\text{m}$, $500 \leq L < 1000 \mu\text{m}$
170 or $\geq 1000 \mu\text{m}$, colour was classified as white-transparent, blue-green, red-yellow or black-grey,
171 and shape was classified as fibre (with a length to diameter ratio exceeding three), film, fragment
172 or spherule-granule.

173 Negative controls, derived by processing 2 x 20 L of filtered water as above and microscopically
174 inspecting the resulting residues revealed no MP contamination arising from the containers or
175 laboratory. Positive controls consisted of ten polyethylene fragments and ten polyvinyl chloride
176 fragments (both white and 20 to 250 μm in diameter sourced from Eppendorf) added, with the aid
177 of tweezers and the microscope, to separate 20-L volumes of filtered water. Processing these
178 controls likewise full recovery in both cases.

179 The most commonly encountered MP types and at least one from each well ($n = 19$ in total) that
180 had been isolated from the groundwater samples were prepared for further characterization.
181 Samples were firstly mounted on conductive copper adhesive tape and analysed for polymeric
182 composition using a micro-Raman spectrometer (LabRAM HR, Horiba, Japan) configured with a

183 laser at 785 nm, a Raman shift of 400-1800 cm^{-1} and acquisition times of 20 to 30 seconds. A high
 184 vacuum scanning electron microscope (SEM; TESCAN Vega 3, Czech Republic) with a resolution
 185 of 2 nm and an accelerating voltage of 20 kV was then used to assess the surface morphology of a
 186 further selection of MPs ($n = 11$) that had been placed on microscope slides and gold-coated.

187

188 **2.3. Modelling rainfall-groundwater lag time**

189 In order to estimate how long it takes rain water and, therefore, any soluble contaminant washed
 190 out from the atmosphere, to reach groundwater, correlograms were generated for eight of the
 191 observation wells shown in Figure 1b according to methods outlined in Samani (2001) and using
 192 data supplied by the Shiraz Regional Water Organization.

193 A correlogram is a plot of the cross-correlation coefficient, $r_{xy}(k)$, as a function of lag, k , and is
 194 defined as follows:

$$195 \quad r_{xy}(k) = \frac{C_{xy}(k)}{\sqrt{C_{xx}(0)C_{yy}(0)}} \quad (1)$$

196 where $C_{xy}(k)$ is the coefficient of cross covariance at lag k for time series $x(t)$ and $y(t)$:

$$197 \quad C_{xy}(k) = \frac{1}{n-k} \sum_{i=1}^{n-k} x_i y_{i+k} - \frac{1}{n^2} \sum_{i=1}^n x_i \sum_{i=1}^n y_i \quad (2)$$

198 and $C_{xx}(0)$ and $C_{yy}(0)$ are the variances at lag zero for x and y , respectively:

199

$$200 \quad C_{xx}(0) = \frac{1}{n} \sum_{i=1}^n (x_i - \bar{x})^2 \quad (3)$$

201

$$202 \quad C_{yy}(0) = \frac{1}{n} \sum_{i=1}^n (y_i - \bar{y})^2 \quad (4)$$

203

204 In the time series of some wells, it was difficult to detect a meaningful relationship between the
205 rainfall and water level because of autocorrelation and data processing was necessary to eliminate
206 or reduce noise. In this context, firstly decomposition of trend and seasonality was applied.
207 Secondly, autoregressive integrated moving average (ARIMA), which is a statistical analysis
208 model using a combination of the differenced autoregressive model with the moving average
209 model, was applied to the residuals arising from the first step to better understand the data set.
210 These steps were continued on the two time series until no trends, patterns or autocorrelation were
211 observed and the cross correlation was applied to the residuals from the ARIMA analysis.

212 All calculations and correlations were performed in Minitab® 16.2.0 and correlograms were
213 generated in Excel 2013. The maximum value of $r_{xy}(k)$ observed in a periodic component of the
214 correlogram was defined as the lag time between rainfall and groundwater level response.

215

216 **3. Results**

217 ***3.1. Quantities and characteristics of microplastics***

218 A selection of MPs identified under the microscope is shown in Figure 2 and the number and
219 nature of MPs detected in the groundwater samples are presented in Table 2. Thus, overall 96 MPs
220 were observed with numbers in individual 20-L samples ranging from 2 (S4) to 26 (S8) (mean =

221 9.8, median = 8.5). The lowest quantities of MP were found in regions relatively remote from
222 urbanization (the Ghalat Mountains in the northwest of the region and towards Maharloo Lake in
223 the southeast). However, the greatest concentrations were not encountered in the vicinity of Shiraz
224 City but were located to the west of the region.

225 Fibres were the dominant MP shape (about 70%), with fragments and films contributing about
226 20% and 10%, respectively. All MPs detected were $\leq 500 \mu\text{m}$ in size, with abundance increasing
227 with decreasing size range and about 60% of MPs encountered below $100 \mu\text{m}$. Although MPs were
228 encountered in all colour categories, black-grey and red-yellow were most common overall and
229 white-transparent and blue-green were most common for non-fibrous particles.

230

231 Table 2: Numbers, categories (by shape) and characteristics (colour and size, where L = longest
 232 dimension or length) of the MPs retrieved from the ten groundwater samples whose locations are
 233 shown in Figure 1.

location or category	fibres	films	fragments	total
S1	1		2	3
S2	6	1	5	12
S3	6	1		7
S4	21	3	2	26
S5	7		3	10
S6	12		1	13
S7	3		2	5
S8	2			2
S9	5	4	4	13
S10	5			5
total	68	9	19	96
$L \leq 100 \mu\text{m}$	41	3	12	56
$100 < L \leq 250 \mu\text{m}$	20	3	7	30
$250 < L \leq 500 \mu\text{m}$	9		1	10
white-transparent	4	3	6	13
blue-green	12	3	5	20
red-yellow	22	2	5	29
black-grey	30	1	3	34

234

235

236

237

238

239

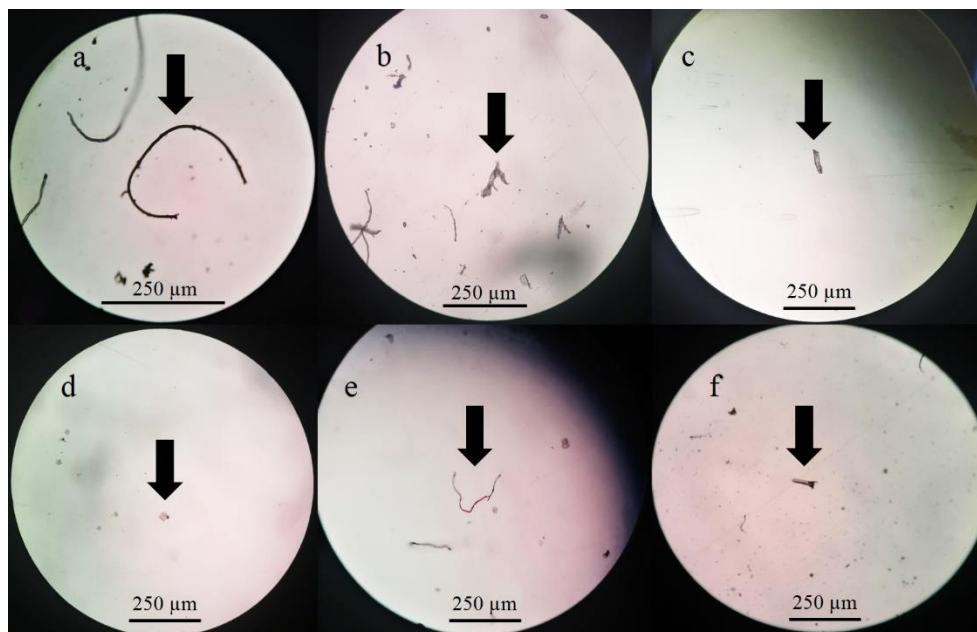
240

241

242

243

244



245 Figure 2: Examples of MP fibres (a and e), fragments (b and f) and films (c and d) retrieved from
246 the groundwater samples and identified under the microscope. Note that much of the remaining
247 material shown, including several additional fibres, was non-plastic.

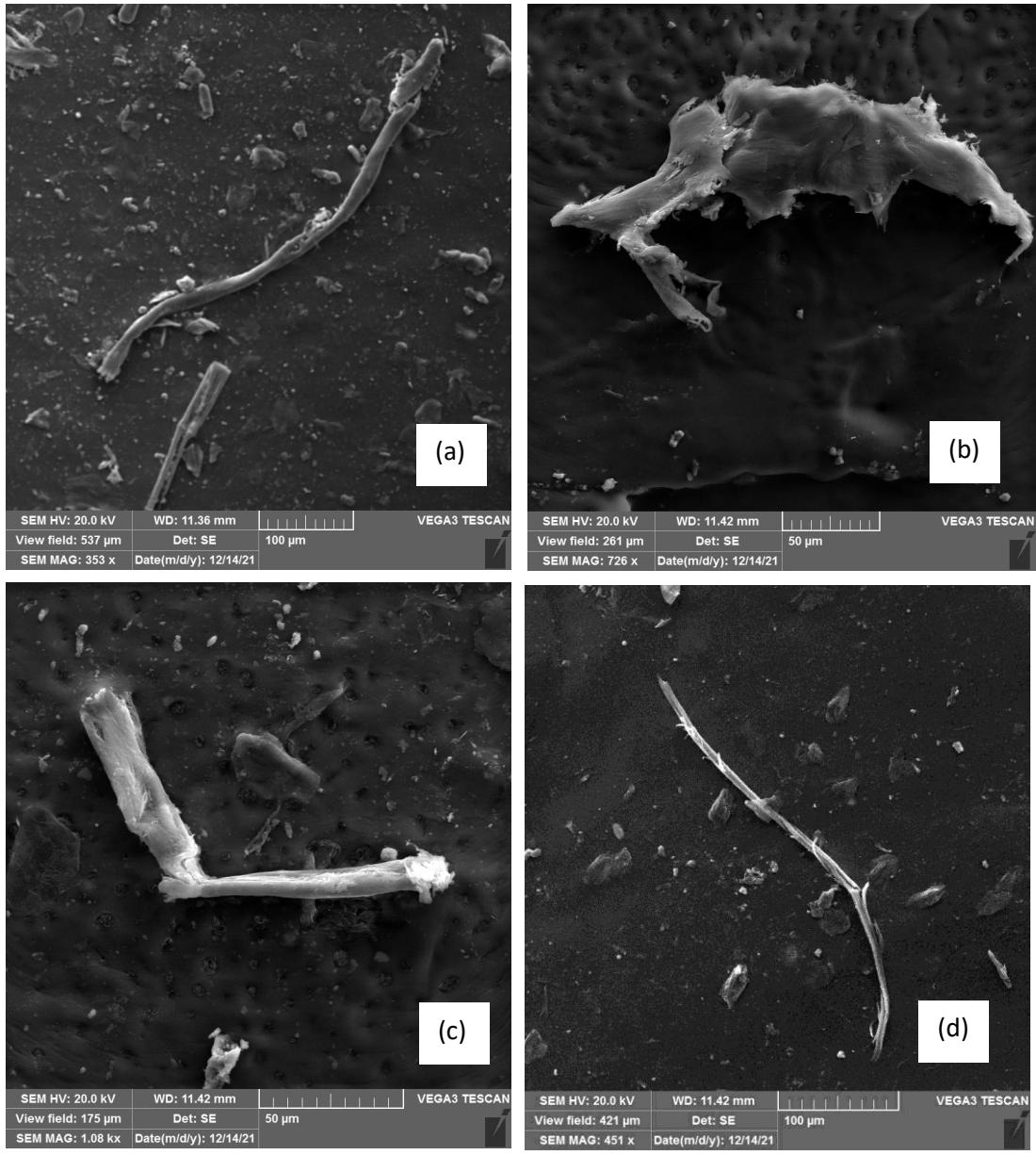
248

249

250

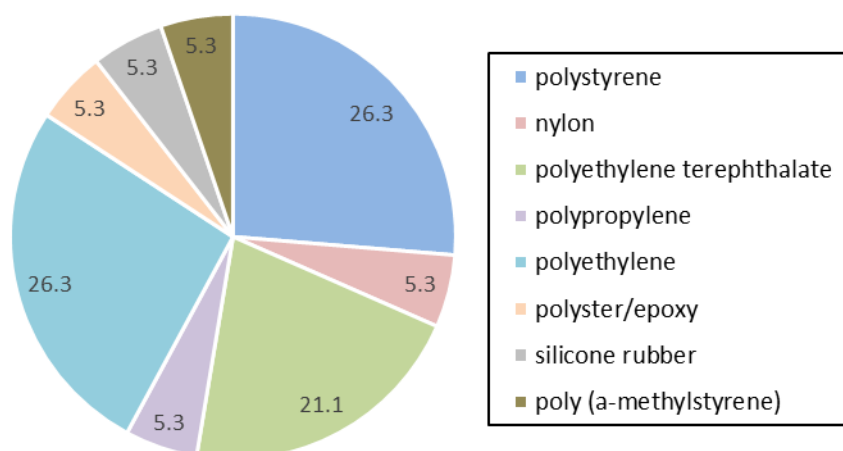
251

252
253
254
255
256
257
258
259
260
261
262
263
264
265
266
267
268
269
270
271
272
273



274 Figure 3: SEM images of three MP fibres (a, c and d) and a film (b) sampled from the
275 groundwater wells.

276 The surfaces of MPs captured by SEM are exemplified in Figure 3. There is evidence of oxidation
277 on the surfaces of some samples (e.g., flaking and pits in Figures 3b and 3c) whereas the surfaces
278 of other MPs appear to be relatively smooth (e.g. Figures 3a and 3d). Physical damage is evident
279 in all cases that includes fracturing, twisting, cleavage and deformation.



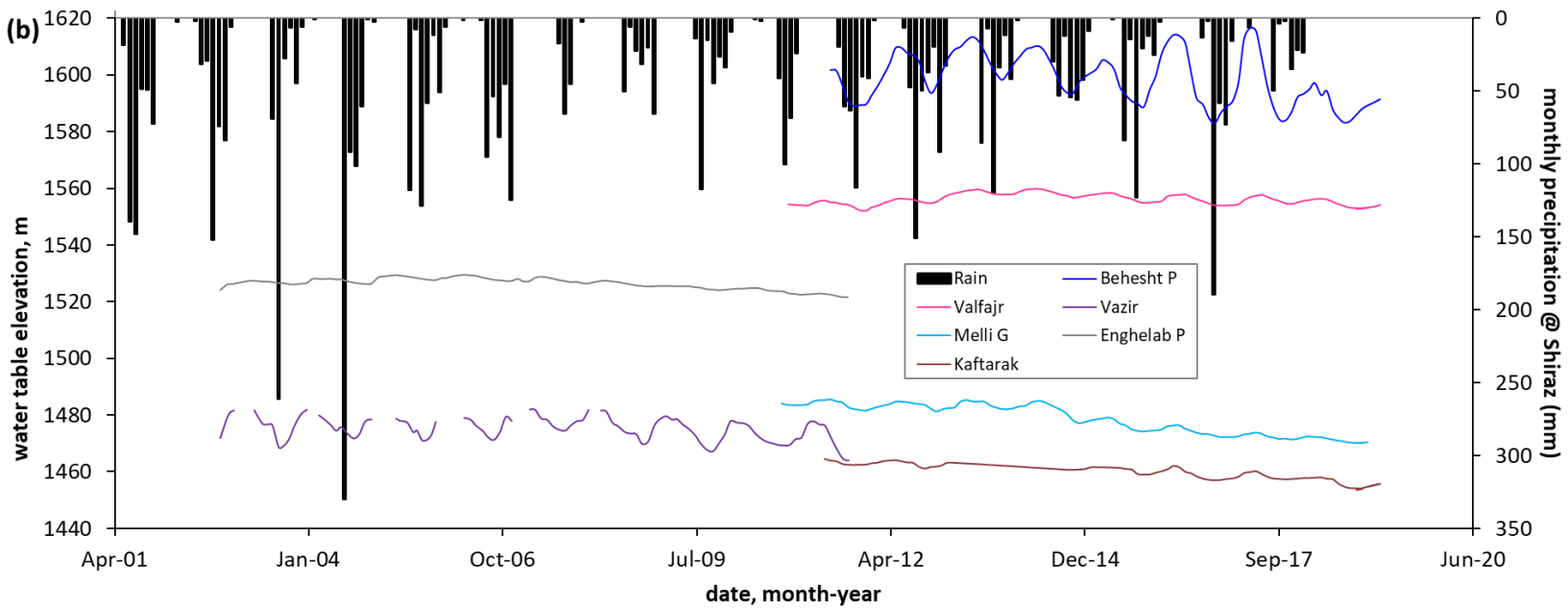
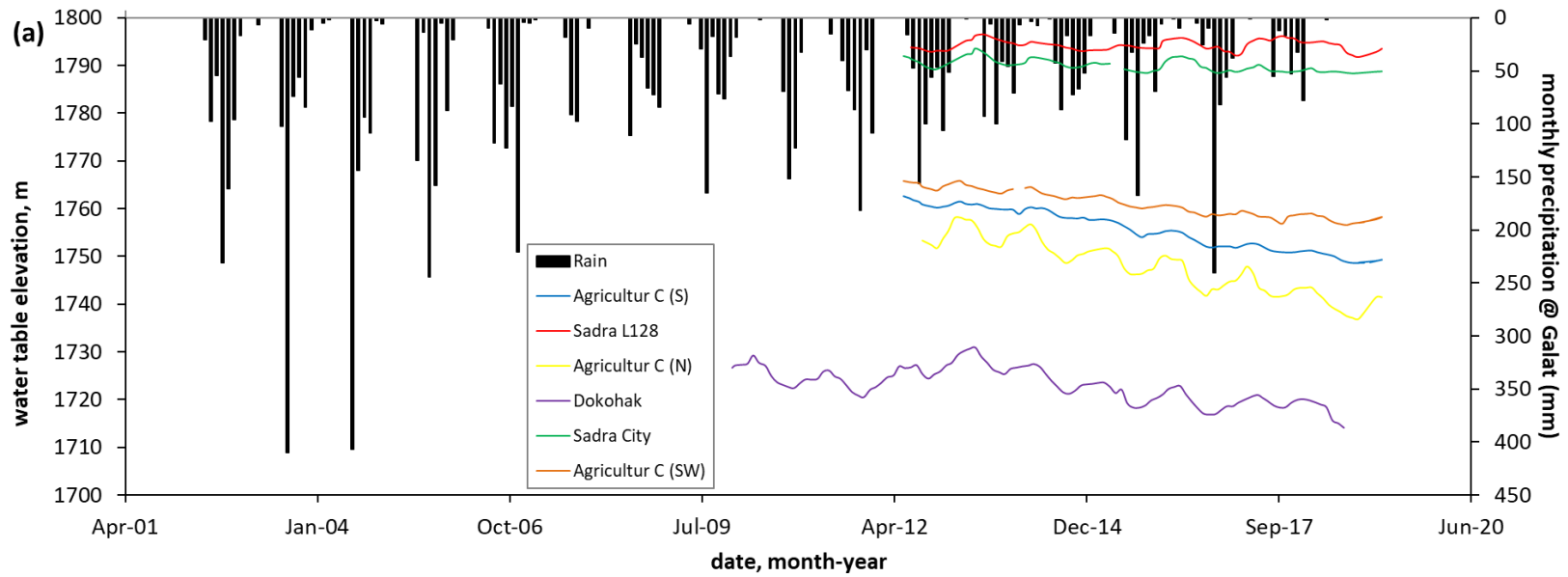
280
281 Figure 4: Percentage distribution of selected MPs ($n = 19$) by polymer type.

282
283 The distribution of selected MPs (~20% in total, and including fibres, fragments and films) is
284 shown by polymer type in Figure 4. More than one-half of MPs were constructed of polystyrene
285 or polyethylene, with an additional sample based on the styrenic compound, poly (α -
286 methylstyrene). Four samples were constructed of polyethylene terephthalate, with four additional
287 polymers or polymer combinations (including a rubber) encountered amongst the remaining
288 samples. These polymers encompass a range of densities from below 1 g cm^{-3} (polyethylene,
289 polypropylene, poly (α -methylstyrene)) to about 1.4 g cm^{-3} (polyester and polyethylene
290 terephthalate). Significantly, only one sample had the same colour and construction as the lining

291 material used in some of the wells (black polyethylene) suggesting that a small degree of
292 contamination from the well structure itself is possible.

293 ***3.2. Meteorological and hydrological data***

294 Monthly rainfall and water table levels, based on available data between 2001 and 2018-2019 held
295 by the Shiraz Regional Water Organization, are plotted as a function of time in Figure 5. Here,
296 water table elevations for six wells to the north of the region are plotted with rainfall data for
297 Ghalat and water table elevations for six wells in the central and southern regions are plotted with
298 rainfall data for Shiraz. At both stations and over the period considered, the seasonality in rainfall
299 is clear and a net reduction in annual rainfall is evident. There is also evidence of an increase in
300 the depth of the water table in many of the time series but rainfall-driven seasonality to this depth
301 is also evident in most cases.



303 Figure 5: Temporal distribution of monthly rainfall and water table level for twelve named
304 observation wells (six using Ghalat precipitation data and six using Shiraz precipitation data).

305

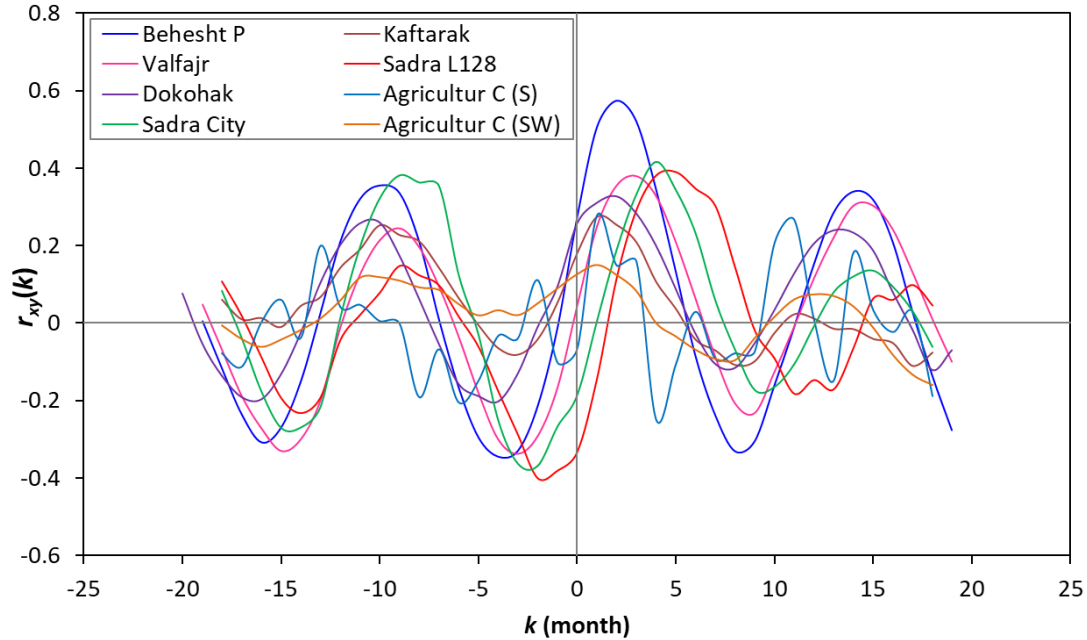
306 **3.3. Cross correlograms and lag time estimation**

307 The cross-correlograms arising from the rainfall and water table data for eight observation wells
 308 is shown in Figure 6. Oscillations with negligible damping indicate the presence of a periodic
 309 component in the total data set and the value of k where $r_{xy}(k)$ is a maximum (the central peak for
 310 each correlogram) provides an estimate of the time lag between rainfall and its intrusion into
 311 groundwater (Samani et al., 2001). Values of k are shown for each well considered in Table 3 and
 312 indicate lags of between one and five months. Note, however, that the three estimates for one
 313 month are associated with the greatest uncertainties (lowest cross-correlation coefficients and least
 314 distinctive central peaks). Overall, there is no clear spatial pattern or statistical relationship with
 315 water table depth, with the greatest time lags (towards the north of the region) associated with the
 316 highest elevations but not the lowest water table depths. Presumably, distributions are dependent
 317 on additional factors such as the precise granulometry of Quaternary deposits, proximity to specific
 318 geological features and the abundance and nature of any impervious surfaces and drainage
 319 systems.

320

321 Table 3: Coordinates, elevations and mean water table (WT) depths for the wells used to
 322 generate the correlograms, and cross-correlation coefficients ($r_{xy}(k)$) and estimates of lag time (k)
 323 derived from the plots in Figure 6.

Location	X	Y	elevation, m	WT depth, m	rainfall data	$r_{xy}(k)$	k , months
Behesht P	642582	3286229	1649	54	Shiraz	0.575	2
Valfajr	640950	3276187	1583	28	Shiraz	0.380	3
Dokohak	635239	3298122	1811	91	Galat	0.382	2
Sadra City	645008	3297135	1813	23	Galat	0.417	4
Kaftarak	663501	3273019	1470	16	Shiraz	0.274	1
Sadra L128	648077	3295764	1819	24	Galat	0.390	5
Agricultur C (S)	652372	3290516	1787	39	Galat	0.278	1
324 Agricultur C (SW)	650875	3292055	1786	30	Galat	0.151	1



325

326

327 Figure 6: Cross-correlograms (cross-correlation coefficient, $r_{xy}(k)$, as a function of lag, k) for
 328 rainfall and water table level at eight observation wells.

329

330 4. Discussion

331 The concentrations of MPs detected on a number basis in groundwater of Shiraz range from 0.1 to
 332 1.3 MP L^{-1} (mean and median = 0.48 and 0.43 MP L^{-1} , respectively). These are lower than
 333 concentrations reported for wells and springs sampled from a more open and creviced karst aquifer
 334 in Illinois (up to 15 MP L^{-1} ; Panno et al., 2019) and are considerably lower than concentrations of
 335 recently reported for unconfined alluvial aquifers in Victoria, Australia (16 to 97 MP L^{-1} ;
 336 O'Connor et al., 2019). Concentrations in the present study are, however, higher than those
 337 reported for groundwater from five of regions of Germany (up to 0.007 MP L^{-1} ; Mintenig et al.
 338 2019) and abstracted from chalk and sandstone aquifers in the UK after treatment by disinfection
 339 or filtration (up to 0.0107 MP L^{-1} ; Johnson et al., 2020). Presumably, these differences reflect

340 variations in hydrogeology, land use, MP sources, means of MP sampling and identification
341 (including size detection limits), and the presence or nature of any water treatment. We also note
342 that, consistent with our observations, Johnson et al. (2020) report polystyrene as the most
343 abundant polymer type, despite the relatively small demand for this plastic compared with
344 polyolefins (Andrady and Neal, 2009).

345 A more useful, quantitative comparison of MPs in Shiraz groundwater is with MPs in precipitation
346 from the same region that have been collected and processed by similar protocols. Thus, according
347 to Abbasi and Turner (2021), concentrations of MPs in monthly precipitation identified
348 microscopically after sample peroxidation are 150 to 2220 MP L⁻¹ (mean = 280 MP L⁻¹; median =
349 75 MP L⁻¹) in Shiraz City and 30 to 680 MP L⁻¹ (mean = 84 MP L⁻¹; median = 15 MP L⁻¹) in the
350 mountains to the northwest. Despite concentrations in Shiraz groundwater being two or three
351 orders of magnitude lower than concentrations in local precipitation, the particle size distributions
352 are similar with the largest contributions to each sample type arising from the $\leq 100 \mu\text{m}$ fraction.

353 Once precipitation encounters the ground it will interact with additional MPs deposited during dry
354 episodes; in the present setting, extended (seasonal) periods of dry weather may allow considerable
355 accumulation of MPs on porous and rough surfaces, with initial rainfall acting to “flush” MPs
356 through water film expansion-release (O’Connor et al., 2019). In agricultural soils, additional MPs
357 may also be introduced through the application of plastic-based mulches (Huang et al., 2020),
358 biosolids used as fertilizers (Crossman et al., 2020) and contaminated irrigation waters (Liu et al.,
359 2018; Kumar et al., 2020), with measurements in the region of Shiraz revealing an average of about
360 0.5 MP per g of surface and subsurface soil (Rezaei et al., 2022). A proportion of precipitation,
361 coupled with any irrigation water, will infiltrate permeable surfaces with its loading of MPs. This
362 load will be modified by the capture or adhesion and retention of MPs in the substrate and,

363 possibly, the remobilization of previously captured particles by the lower ionic strength of
364 percolating rainwater (Goepfert and Goldscheider, 2021). A reduction in MP concentration from
365 precipitation to groundwater observed in the present study suggests significant net removal during
366 infiltration.

367 Variations in MP concentrations observed in groundwater throughout the region reflect variations
368 in dry and wet deposition rates, land use (including application of irrigation water), surface
369 permeability and infiltration rates, underlying geology and granulometry, and depth of the water
370 table. For instance, one of the lowest MP concentrations was encountered in the remote and most
371 elevated region of the Ghalat Mountains (S1) where plastic deposition is, presumably, minimal,
372 and the mean water table is located at about 180 m below the surface; under these conditions, the
373 concentration of MPs serve as a regional baseline. The highest concentrations of MPs were
374 encountered to the west of Shiraz City (S4 and S6) where MP inputs are augmented by agricultural
375 activities (including use of urban waste waters for irrigation; Rezaei et al., 2022), infiltration is
376 promoted by extensive ploughing, and the vertical transport of groundwater is expedited by the
377 Sabz Pushan fault (Lacombe et al., 2006). Samples from the most populated and industrialized
378 districts of Shiraz City itself (S5 and S10) exhibit moderate concentrations of MPs, despite a
379 multitude of sources of MPs in the urban setting (Abbasi et al., 2017; Grbic et al., 2020). This may
380 be attributed to the abundance of impermeable surfaces (roads and buildings) that limit exchange
381 with the subsurface environment.

382 The MPs retrieved from the wells of the Shiraz aquifer are irregular in shape (and mainly fibrous)
383 and degree of weathering, and are heterogeneous in polymer makeup and density (including both
384 positively and negatively buoyant particles). It is surmised that those sampled reflect a
385 combination of MPs that have migrated vertically from the surface to the water table, and taking

386 at least one to five months to do so depending on the geological, hydrological and land-use factors
387 described above, and those that have, additionally, been transported along the gradient of the water
388 table. Based on a median hydraulic conductivity for Shiraz aquifer of 12 m d^{-1} (Baghapour et al.,
389 2016), a hydraulic gradient ranging from 0.006 in the alluvial fans to 0.001 in the vicinity of the
390 Maharloo Lake (Tajabadi et al., 2018) and a transmissivity of $86.4 \text{ m}^2 \text{ d}^{-1}$ (Masoomi, 2016),
391 groundwater flows and flow velocities are estimated to be between 0.09 and $0.6 \text{ m}^3 \text{ d}^{-1}$ and about
392 0.01 and 0.07 m d^{-1} , respectively.

393 While the hydraulic timescales referred to above define the periods involved in the vertical and
394 lateral diffusive transportation of soluble contaminants, it would be expected that MPs are impeded
395 through physical, hydrophobic and, if sufficiently oxidized, chemical and electrostatic interactions
396 with the substrate. O'Connor et al. (2019) studied the vertical migration of polyolefin-based
397 plastics of diameter $21\text{-}535 \text{ }\mu\text{m}$ in sand-soil columns subject to different environmental conditions.
398 Migration was greatest for the finest MPs but was predicted to be limited to a few m over many
399 years. In contrast, at a large-scale alluvial aquifer test site, Goepfert and Goldscheider (2021)
400 found that polystyrene spheres below $5 \text{ }\mu\text{m}$ in diameter travelled up to 200 m along a natural
401 gradient and at velocities up to 6.25 m h^{-1} and, in many cases, more quickly than the diffusion of
402 a tracer solute. These, field-based observations suggest that retardation and filtration are not
403 necessarily important for very fine, regularly-shaped MPs.

404 There are no direct data available on the movement of more irregularly-shaped MPs, like fibres,
405 in soils. However, a general theoretical framework that is applicable to large fibre-like colloids
406 was presented by Engdahl (2018). Here, the physical filtration of massless, non-interacting fibres
407 of constant length (and treated as bead-rod chains) was simulated through a poorly consolidated,
408 coarse-grained alluvial deposit (mean pore water velocity = 26 m d^{-1}) using a “random obstacle

409 model". The shortest fibres considered (~ 1.3 mm) were smaller than the average pore size of the
410 medium and could be transported unimpeded as they readily aligned with the velocity field. These
411 fibres could also progress more quickly than a passive tracer because of their ability to bypass slow
412 moving regions. Longer fibres (up to 3.3 mm) were subject to bending, flipping and rolling and
413 were more readily retarded by wrapping around grains. Simulations performed at lower speeds
414 exhibited less retardation than faster simulations and in each case the magnitude of the filtration
415 speed was proportional to the length of the fibre.

416 Based on experimental observations and theoretical simulations, and neglecting any interactions
417 arising from friction, flocculation and electrostatics, the slow velocity fields of the Shiraz aquifer
418 are predicted to favour the transport of regularly-shaped MPs and fibres that are smaller (or shorter)
419 than the mean pore size of the medium, including those evading detection in our analysis, with
420 larger MPs impeded by physical constraints. Regardless of the degree of retardation, however, the
421 flow velocities involved across the 50 km northwest-southeast axis of the Shiraz aquifer suggest
422 that MPs may reside in the system for years to decades, hampering any clear means of source
423 identification.

424

425 **5. Conclusion**

426 The present study is the first to document the presence, concentrations and characteristics of MPs
427 in an aquifer from a semi-arid region, and only the second to report MPs in an alluvial groundwater
428 system. MP concentrations are heterogeneous throughout the Shiraz aquifer and range from 0.1 to
429 1.3 MP L⁻¹, with fibres $\leq 500 \mu\text{m}$ in length the dominant shape and polyethylene, polystyrene and
430 polyethylene terephthalate the most important polymers. MP heterogeneity is attributed to

431 different land-uses, including variable agricultural practices, and variations in local geology,
432 permeability and infiltration rates. Based on time lags between precipitation and intrusion into the
433 aquifer, groundwater flow rates and retardation of fine particulate material in porous media, we
434 predict that MPs are likely to reside in the Shiraz aquifer system for years to decades. Nevertheless,
435 because groundwater is frequently used as a supply of potable water, its consumption may make
436 to a contribution to human exposure through ingestion.

437

438 **Acknowledgements**

439 We thank Shiraz University for funding the study (grant no. 99GRC1M371631).

440

441 **References**

442 Abbasi, S., Turner, A., 2021. Dry and wet deposition of microplastics in a semi-arid region
443 (Shiraz, Iran). *Science of the Total Environment* 786, 147358.

444 Abbasi, S., Keshavarzi, B., Moore, F., Delshab, H., Soltani, N., Sorooshian, A., 2017.
445 Investigation of microrubbers, microplastics and heavy metals in street dust: a study in Bushehr
446 city, Iran. *Environmental Earth Sciences* 76, 798.

447 Abd-Elhamid, H.F., Abd-Elmoneem, S.M., Abdelaal, G.M., Zelenáková, M., Vranayova, Z.,
448 Abd-Elaty, I., 2021. Investigating and managing the impact of using untreated wastewater for
449 irrigation on the groundwater quality in arid and semi-arid regions. *Int. J. Environ. Res. Public*
450 *Health* 18, 7485. <https://doi.org/10.3390/ijerph18147485>

451 Abdesselam, S., Halitim, A., Jan, A., Troland, F., Bourrié, G., 2013. Anthropogenic
452 contamination of groundwater with nitrate in arid region: case study of southern Hodna
453 (Algeria). *Environmental Earth Sciences* 70, 2129-2141.

454 Andrady, A.L., Neal, M.A., 2009. Applications and societal benefits of plastics. *Philosophical*
455 *Transactions of the Royal Society of London B: Biological Sciences* 364, 1977-1984.

456 Allen, S., Allen, D., Phoenix, V.R., Le Roux, G., Jimenez, P.D., Simonneau, A., Binet, S.,
457 Galop, D., 2019. Atmospheric transport and deposition of microplastics in a remote mountain
458 catchment. *Nature Geoscience* 12, 339-344.

459 Charizopoulos, N., Zagana, E., Psilovikos, A., 2018. Assessment of natural and anthropogenic
460 impacts in groundwater, utilizing multivariate statistical analysis and inverse distance weighted
461 interpolation modeling: the case of a Scopia basin (Central Greece). *Environmental Earth*
462 *Sciences* 77, article no. 380.

463 Coyle, R., Hardiman, G., O'Driscoll, K., 2021. Microplastics in the marine environment: A
464 review of their sources, distribution processes, uptake and exchange in ecosystems. *Case Studies*
465 *in Chemical and Environmental Engineering* 2, 100010.

466 Crossman, J., Hurley, R.R., Futter, M., Nizzetto, L., 2020. Transfer and transport of
467 microplastics from biosolids to agricultural soils and the wider environment. *Science of the Total*
468 *Environment* 724, 138334.

469 da Costa, P.J., Paço, A., Santos, P.S.M., Duarte, A.C., Rocha-Santos, T., 2018. Microplastics in
470 soils: assessment, analytics and risks. *Environmental Chemistry* 16, 18–30.

471 De Witte, B.; Devriese, L.; Bekaert, K.; Hoffman, S.; Vandermeersch, G.; Cooreman, K.;
472 Robbens, K., 2014. Quality assessment of the blue mussel (*Mytilus edulis*): Comparison between
473 commercial and wild types. *Marine Pollution Bulletin* 85, 146-155.

474 El Alfy, M., Faraj, T., 2016. Spatial distribution and health risk assessment for groundwater
475 contamination from intensive pesticide use in arid areas *Environmental Geochemistry and Health*
476 39, 231-253.

477 Engdahl, N.B., 2018. Simulating the mobility of micro-plastics and other fiber-like objects in
478 saturated porous media using constrained random walks. *Advances in Water Resources* 121,
479 277-284.

480 Fernández-Cirelli, A., Arumí, J.L., Rivera, D., Boochs, P.W., 2009. Environmental effects of
481 irrigation in arid and semi-arid regions. *Chilean Journal of Agricultural Research* 69, 27-40.

482 Goepfert, N., Goldscheider, N., 2021. Experimental field evidence for transport of microplastic
483 tracers over large distances in an alluvial aquifer. *Journal of Hazardous Materials* 408, 124844.

484 Grbic, J., Helm, P., Athey, S., Rochman, C.M., 2020. Microplastics entering northwestern Lake
485 Ontario are diverse and linked to urban sources. *Water Research* 174, 115623.

486 Hidalgo-Ruz, V.; Gutow, L.; Thompson, R.C.; Thiel, M., 2012. Microplastics in the marine
487 environment: A review of the methods used for identification and quantification. *Environmental*
488 *Science & Technology* 46, 3060-3075.

489 Hssaisoune, M., Bouchaou, L., Sifeddine, A., Bouimetarhan, I., Chehbouni, A., 2020. Moroccan
490 groundwater resources and evolution with climate changes. *Geosciences* 10, 81;
491 doi:10.3390/geosciences10020081

492 Huang, Y., Liu, Q., Jia, W., Yan, C., Wang, J., 2020. Agricultural plastic mulching as a source of
493 microplastics in the terrestrial environment. *Environ. Pollut.* 260, 114096.
494 <https://doi.org/10.1016/j.envpol.2020.114096>.

495 Johnson, A.C., Ball, H., Cross, R., Horton, A.A., Jürgens, M.D., Read, D.S., Vollertsen, J.,
496 Svendsen, C., 2020. Identification and quantification of microplastics in potable water and their
497 sources within water treatment works in England and Wales. *Environmental Science and*
498 *Technology* 54, 12326-12334.

499 Kumar, M., Xiong, X., He, M., Tsang, D.C.W., Gupta, J., Khan, E., Harrad, S., Hou, D., Ok,
500 Y.S., Bolan, N.S., 2020. Microplastics as pollutants in agricultural soils. *Environmental Pollution*
501 265, 114980.

502 Lacombe, O., Mouthereau, F., Kargar, S., Meyer, B., 2006. Late Cenozoic and modern stress
503 fields in the western Fars (Iran): Implications for the tectonic and kinematic evolution of central
504 Zagros. *Tectonics* 25, TC1003.

505 Li P., Karunanidhi, D., Subramani, T., Srinivasamoorthy, K., 2021. Sources and consequences of
506 groundwater contamination. *Archives of Environmental Contamination and Toxicology* 80, 1-10.

507 Liu, M., Luo, S., Yang, S., Lei, L., Hu, J., Lv, W., Zhou, W., Cao, C., Shi, H., Yang, X., He, D.,
508 2018. Microplastic and mesoplastic pollution in farmland soils in suburbs of Shanghai, China.
509 *Environ. Pollut.* 242, 855–862.

510 Masoomi, B., 2016. Estimation of hydraulic parameters of Shiraz plain unconfined aquifer using
511 Aquifer Test software. *The Second International Conference on New Research Findings in*
512 *Science, Engineering and Technology*.

513 Mintenig, S.M., Loder, M.G.J., Pringle, S., Gerdt, G., 2019. Low numbers of microplastics
514 detected in drinking water from ground water sources. *Science of the Total Environment* 648,
515 631-635.

516 Ng, E. L., Lwanga, E. H., Eldridge, S. M., Johnston, P., Hu, H. W., Geissen, V., Chen, D., 2018.
517 An overview of microplastic and nanoplastic pollution in agroecosystems. *Science of the Total*
518 *Environment* 627, 1377-1388.

519 O'Connor, D., Pan, S., Shen, Z., Song, Y., Jin, Y., Wu, W.M., Hou, D., 2019. Microplastics
520 undergo accelerated vertical migration in sand soil due to small size and wet-dry cycles.
521 *Environmental Pollution* 249, 527-534.

522 Oren, O., Yechieli, Y., Böhlke, J.K., Dody, A., 2004. Contamination of groundwater under
523 cultivated fields in an arid environment, central Arava Valley, Israel. *Journal of Hydrology* 290,
524 312-328.

525 Panno, S.V., Kelly, W.R., Scott, J., Zheng, W., McNeish, R.E., Holm, N., Hoellein, T.J.,
526 Baranski, E.L., 2019. Microplastic contamination in karst groundwater systems. *Groundwater*
527 *57*, 189-196.

528 Rezaeia, M., Abbasi, S., Oleszczuk, P., Pourmahmoodd, H., Ritsema, C., Turner, A., 2022.
529 Microplastics in agricultural soils and their transport by wind erosion. Submitted.

530 Rodríguez-Estrella, T., 2012. The problems of overexploitation of aquifers in semi-arid areas: the
531 Murcia Region and the Segura Basin (South-east Spain) case. *Hydrology and Earth System*
532 *Science Discussions 9*, 5729-5756.

533 Samandra, S., Johnston, J.M., Jaeger, J.E., Symons, B., Xie, S., Currell, M., Ellis, A.V., Clarke,
534 B.O., 2022. Microplastic contamination of an unconfined groundwater aquifer in Victoria,
535 Australia. *Science of the Total Environment 802*, 149727.

536 Samani, N., 2001. Response of karst aquifers to rainfall and evaporation, Maharlu Basin, Iran.
537 *Journal of Cave and Karst Studies 63*, 33-40.

538 Scanlon, B.R., Keese, K.E., Flint, A.L., Flint, L.E., Gaye, C.B., Edmunds, W.M., Simmers, I.,
539 2006. Global synthesis of groundwater recharge in semiarid and arid regions *Hydrological*
540 *Processes 20*, 3335-3370.

541 Tanentzap, A.J., Cottingham, S., Fonvielle, J., Riley, I., Walker, L., Woodman, S.G., Kontou, D.,
542 Pichler, C.M., Reisner, E., Lebreton, L., 2021. Microplastics and anthropogenic fibre
543 concentrations in lakes reflect surrounding land use. *PLoS Biol 19*, e3001389.
544 <https://doi.org/10.1371/journal.pbio.3001389>

545

546